HAL
open science

Double-Lattice Packing of Pentagonal Gold Bipyramids in Supercrystals with Triclinic Symmetry

Jieli Lyu, Wajdi Chaâbani, Evgeny Modin, Andrey Chuvilin, Thomas Bizien, Frank Smallenburg, Doru Constantin, Marianne Impéror-Clerc, Cyrille Hamon

To cite this version:

Jieli Lyu, Wajdi Chaâbani, Evgeny Modin, Andrey Chuvilin, Thomas Bizien, et al.. Double-Lattice Packing of Pentagonal Gold Bipyramids in Supercrystals with Triclinic Symmetry. Advanced Materials, 2022, pp.2200883. 10.1002/adma.202200883 . hal-03648507

HAL Id: hal-03648507

https://hal.science/hal-03648507v1

Submitted on 21 Apr 2022

HAL is a multi-disciplinary open access archive for the deposit and dissemination of scientific research documents, whether they are published or not. The documents may come from teaching and research institutions in France or abroad, or from public or private research centers.

L'archive ouverte pluridisciplinaire **HAL**, est destinée au dépôt et à la diffusion de documents scientifiques de niveau recherche, publiés ou non, émanant des établissements d'enseignement et de recherche français ou étrangers, des laboratoires publics ou privés.

Double-lattice packing of pentagonal gold bipyramids in supercrystals with triclinic symmetry

Jieli Lyu,[1] Wajdi Chaabani,[1] Evgeny Modin,[2] Andrey Chuvilin,[2,3] Thomas Bizien,[4] Frank Smallenburg,[1] Marianne Impéror-Clerc,[1]* Doru Constantin,[5]* Cyrille Hamon[1]**

[1] Université Paris-Saclay, CNRS, Laboratoire de Physique des Solides, 91405 Orsay, France.

[2] Electron Microscopy Laboratory, CIC NanoGUNE BRTA, Tolosa Hiribidea, 76, 20019 Donostia – San Sebastian, Spain.

[3] Basque Foundation of Science, IKERBASQUE, 48013 Bilbao, Spain.

[4] SWING beamline, SOLEIL Synchrotron, Gif-sur-Yvette, France.

[5] Institut Charles Sadron, CNRS and Université de Strasbourg, 67034 Strasbourg, France.

KEYWORDS: Supercrystal; Small angle X-Ray scattering; Evaporation-induced self-assembly; FIB-SEM tomography; Surface enhanced Raman scattering; Gold nanoparticles.

E-mail: frank.smallenburg@universite-paris-saclay.fr, marianne.imperor@universite-paris-saclay.fr, constantin@unistra.fr, cyrille.hamon@universite-paris-saclay.fr

Abstract

Pentagonal packing is a long-standing issue and a rich mathematical topic, brought to the fore by recent progress in nanoparticle design. Gold pentagonal bipyramids combine five-fold symmetry and anisotropy and their section varies along the length. In this work, we obtain colloidal supercrystals of pentagonal gold bipyramids in a compact arrangement that generalizes the optimal packing of regular pentagons in the plane. Multimodal investigations reveal a two-particle unit cell with triclinic symmetry, a lower symmetry than that of the building blocks. Monte Carlo computer simulations show that this lattice achieves the densest possible packing. Going beyond pentagons, further simulations show an odd-even effect of the number of sides on the packing: odd-sided bipyramids are non-centrosymmetric and require the double-lattice arrangement to recover inversion symmetry. The supercrystals display a facet-dependent optical response that is promising for sensing, metamaterials applications and for fundamental studies of self-assembly processes.

Introduction

Since Greek antiquity, scientists have been fascinated by the way identical bodies pack together in regular assemblies. Determining their optimal packing, i.e. the one with the highest possible volume fraction is still a challenging task, even for bodies with simple geometrical shapes like convex polyhedra or polygons in the plane. Recently, this quest for optimal packing has been fueled by the design of nanoparticles with increased structural complexity, which typically self-assemble into dense supercrystals. However, the vast majority of these efforts have focused on isometric particles (with a similar size along the three space directions)[1] and elongated shapes have received much less attention.[2]

Fivefold symmetry is ubiquitous, from human-made architecture to floral symmetries.[3] In two dimensions, pentagonal packing is a long-standing issue and a rich mathematical topic, started by the early work of Johannes Kepler.[4] Tiling the plane with pentagons can be achieved either with non-regular pentagons in 15 different ways[5] or in combination with other polygonal shapes, giving rise to the fascinating aperiodic Penrose tilings.[6] The optimal packing of regular pentagons is a periodic lattice with a packing fraction around 0.92 called the 'pentagonal ice ray'.[7] First reported in China as a decorative pattern,[8] it consists of two vertical columns of pentagons pointing in opposite direction and stacked along their edges.[7] Since the two orientations of pentagons form two sublattices that are related to each other via an inversion center, this results in a double-lattice packing.[9] This organization has also been observed in numerical simulations of hard pentagons.[10]

Fivefold symmetry is regularly encountered in the shape of gold nanoparticles (NPs), as a result of crystal twinning during particle synthesis. For instance, gold bipyramids consist of two pentagonal pyramids base-stacked together.[11] Pentatwinned gold bipyramids were first obtained as a byproduct in gold nanorod synthesis,[12] but since then high-yield synthesis has been achieved by seed-mediated growth.[13] The self-assembly of pentagonal bipyramids has

been studied within monolayers,[14] but their self-assembly into 3D supercrystals has not yet been elucidated. In contrast to many other elongated particles, the cross-section of a pentagonal bipyramid is not constant along the symmetry axis, and hence their packing in 3D space does not reduce to its two-dimensional counterpart.[2] Allowing the section to vary along the length increases the complexity of the problem, as demonstrated by the case of ellipsoids.[15] For ellipsoids, the unit cell of the densest lattice contains a motif of two inequivalent particles having two different orientations.[16] Although the stacking of ellipsoid-like particles such as bipyramids, prolate spheroids and bicones has been investigated numerically,[1c, 15-17] there is to date no experimental evidence on the three-dimensional packing of elongated particles with varying cross-section. This may be due to their relative experimental scarcity: notable exceptions are hematite nanoparticles[18] and ellipsoidal microparticles,[19] but crystallization also requires a high size and shape homogeneity of the particle ensemble,[20] which was difficult to achieve until about fifteen years ago. Furthermore, investigating the structure of the supercrystals by electron microscopy in real space is challenging, as the electrons typically interact too strongly with the nanoparticles to penetrate the bulk of supercrystals and reveal their three-dimensional order.

In this work, we obtain long-range supercrystals of pentagonal gold bipyramids with a packing fraction of 0.835. Their structure is a double-lattice packing, where all bipyramids are arranged parallel to each other but have two different in-plane orientations of the pentagonal cross-section. This double lattice generalizes the optimal packing of regular pentagons in the plane, the 'pentagonal ice ray', in the sense that the two orientations of the pentagonal bipyramids are related to each other by an inversion center. Synchrotron-based small-angle X-ray scattering (SAXS) and focused ion beam-scanning electron microscopy (FIB-SEM) tomography analysis reveal a two-particle unit cell with triclinic symmetry. Monte Carlo (MC) computer simulations show that this arrangement corresponds to the densest possible packing. The crystalline order

of the bipyramids results in a facet-dependent optical response, which is demonstrated by surface-enhanced Raman scattering (SERS) spectroscopy.

Results and Discussion

Pentatwinned gold bipyramids (AuBPs) were obtained by seed-mediated growth and were uniform in size, as shown by a relative standard deviation of the length and width below 8% (e.g. length: 75.3±3.6 nm, base width: 25.2±1.5 nm). We optimized the conditions to crystallize the AuBPs via the slow evaporation (i.e. 48h) of a sessile droplet, and investigated their nanostructuration. The optical and structural characterization are provided in the Supporting Information (Sections 1 and 2). Results show that not only the detailed shape of the bipyramids matters (anisotropy, truncation of the tips) but also that the surfactant (i.e. hexadecyltrimethylammonium chloride (CTAC)) concentration has to be tuned carefully to obtain supercrystals. **Figure 1** shows a combined SAXS and SEM analysis of a sample comprising AuBPs supercrystals.

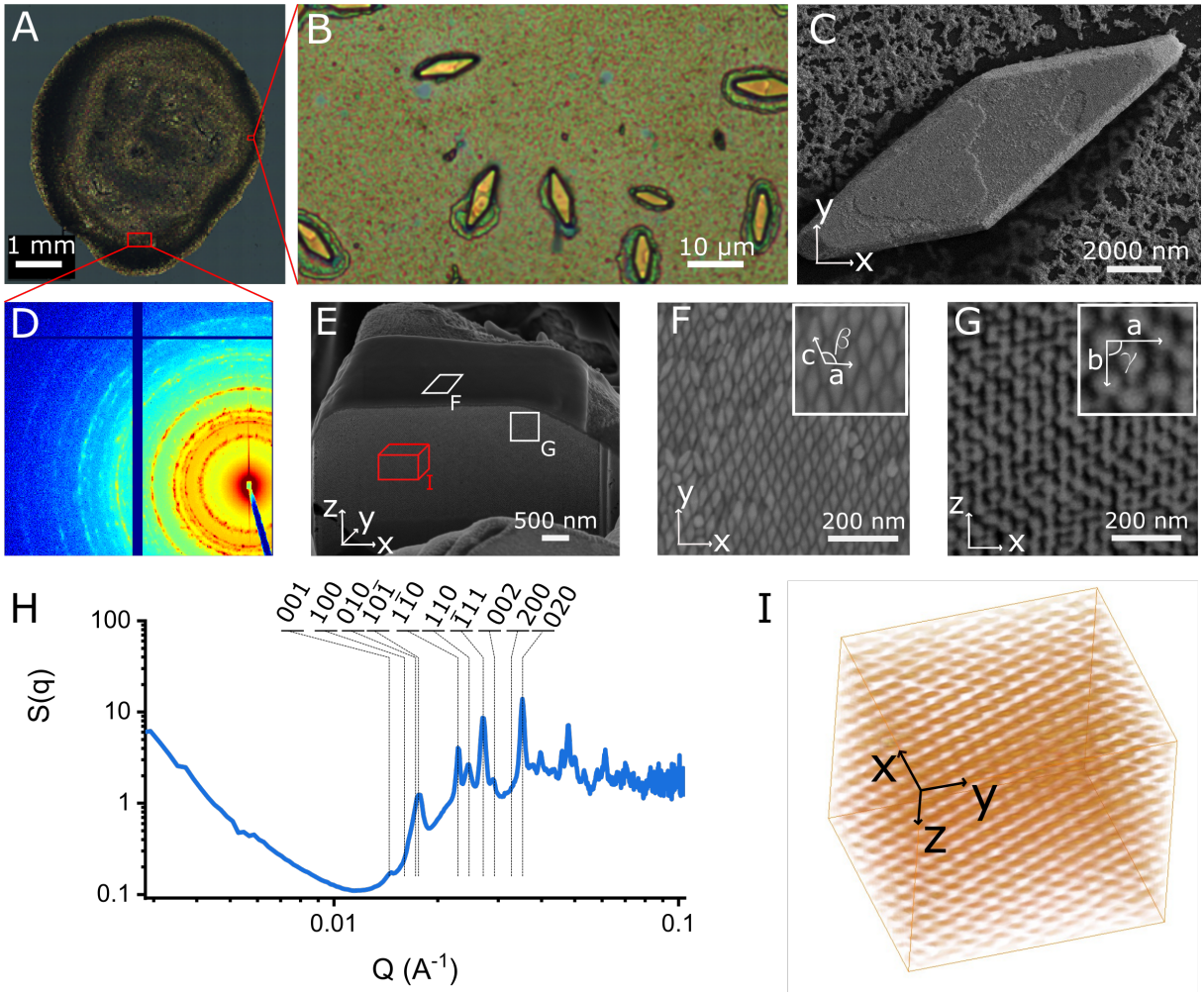

Figure 1: Multiscale characterization of pentagonal gold bipyramid supercrystals obtained by evaporation-induced self-assembly. A-B) Optical microscopy image of rhomboidal supercrystals at different magnifications. C) SEM micrograph of a rhomboidal supercrystal. D) Representative 2D SAXS image, displayed on a logarithmic intensity scale. E-G) SEM micrographs of an AuBP supercrystal viewed at different magnification and different orientations. In E), the supercrystal was sliced by FIB to reveal the NPs' organization from the top (F) and from the side (G). The insets in F, G) shows the lattice parameters *a*, *b*, *c*, *β*, *γ* of the triclinic unit cell. H) SAXS data with experimental structure factor, S(q). Vertical lines indicate the expected positions of some Bragg peaks of the triclinic lattice. I) Three-dimensional reconstruction of a portion of the supercrystal. In SAXS and SEM, 64 mM in Au^0

and 16 mM in Au^0 were used for the preparation of the sample, respectively. A fixed concentration of CTAC of 2.5 mM was used in all cases.

Low-magnification optical microscopy images show numerous supercrystals, a few micrometers in size and with the same rhomboidal shape, scattered randomly on the substrate. In the 2D SAXS image (**Figure 1D**), the assemblies exhibited Bragg spots, indicating the presence of supercrystals within the footprint of the X-ray beam (300x500µm²). We also obtained the structure factor S(q) as the ratio between the intensity scattered by the supercrystal and the one for isolated gold bipyramids. As shown in **Figure 1H**, the Bragg peak positions are in agreement with a triclinic lattice. In order to confirm the lattice symmetry, AuBPs supercrystals were investigated by SEM. Analysis of the surface of the supercrystal revealed that all bipyramids are oriented in the same direction and parallel to the substrate (**Figure 1F**). Further investigation of the internal structure was carried on by FIB-SEM tomography, allowing the 3D rendering of a portion of the supercrystal (**Video S1**).[21] 2D analysis of the images allowed identifying the lattice vectors of the triclinic unit cell (**Figure 1F-G**). 3D analysis of the supercrystal revealed that all layers were identical and were stacked in an ABA fashion, with a relative offset along the 2**c**+**a** triclinic lattice direction. From the SEM image analysis, we confirmed that the supercrystal belongs to the triclinic symmetry, in agreement with the SAXS indexing of the Bragg peaks. Additional SEM images of the sample (in 2D and 3D) are provided in the Supporting Information (Section 4).

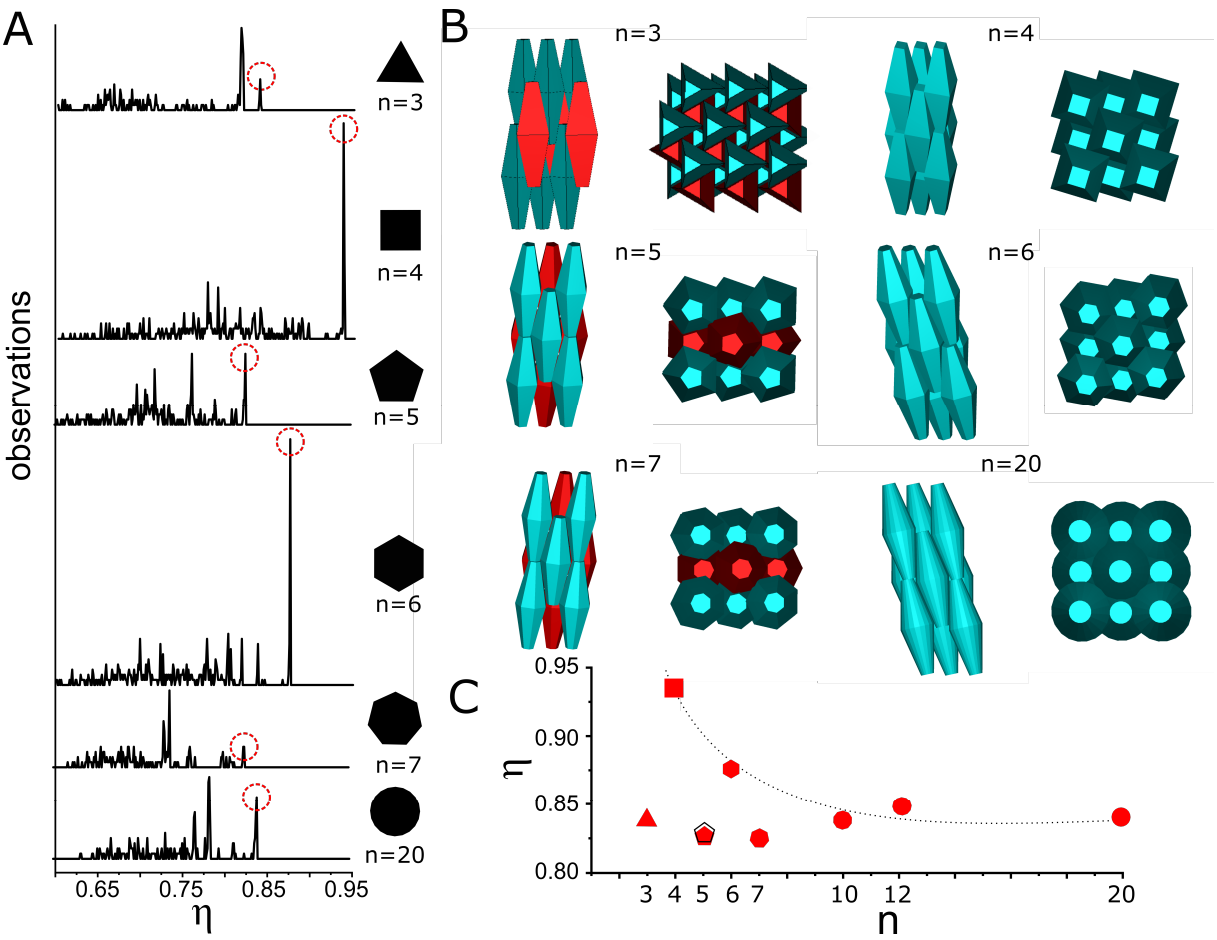

Figure 2: Monte-Carlo computer simulation of the packing of truncated bipyramids with varying cross section. A) Histograms of the packing fraction of predicted phases for n-sided bipyramids with, n=3, n=4, n=5, n=6, n=7 and n=20. B) Representation along two directions of the predicted phase with the highest packing fraction, for each shape, corresponding to the peak highlighted by a red dotted circle in (A). For odd n values, two colors (blue and red) are used as the unit cell is composed of two particles with different orientations. C) Graph representing the packing fraction of the densest phase for each bipyramidal shape as a function of n. The packing fraction determined experimentally (for n=5) is added as an open black pentagon for comparison.

Next, we performed MC computer simulations in order to investigate the effect of the detailed shape of the bipyramids on the lattice symmetry. In particular, we use a crystal structure prediction technique based on MC simulations of small numbers of particles in a simulation

box with a variable shape.[22] Here, we make the assumption that the interactions between the bipyramids are dominated by the hard cores, and neglect other possible interactions due to e.g. charges, Van der Waals attractions, or ligands. Note that since the bipyramids used in this work are large compared to the size of the CTAC ligands, we do not expect the ligands to modify the nature of the interaction. Hence, our model consists of perfectly hard truncated bipyramids, with varying number of vertices on the polygonal base: n= 3, 4, 5, 6, 7, 10, 12 and 20. For each particle shape, we simulate on the order of 300 compression runs, in which a small variable unit cell containing between 2 and 6 particles is compressed slowly under gradually increasing pressure. After compression, we examine the final structures and calculate their packing fractions. In practice, structures that are commonly found using this method tend to be good candidates for entropically favored phases in the system, and the densest-packed phase is expected to be the stable phase at sufficiently high packing fractions.[22-23] Note that the anisotropy and the truncation of the object are closed to the ones obtained experimentally and, if these parameters were varied, the simulation outcome would change, especially if the anisotropy decreased significantly. We show the results of the simulations in histograms of the number of observations of predicted structures as a function of packing fraction, together with two snapshots of the corresponding densest structure (**Figure 2A-B**). Interestingly, five recurrent structures were found for n=5, but only one for both n=4 and n=6 and at most three for the other shapes. For n=4 and n=6, the packing fraction of the predicted structure was about 0.94 and 0.87 respectively. For n=5, the packing fraction of the recurrent structures varied between 0.69 and 0.83 (**Figure 2A**). In **Figure 2C**, we plotted the packing fraction of the densest recurrent structure as a function of n. For n<10, results show an odd-even effect of the number of sides on the packing density: bipyramids with an odd number of vertices yield less dense structures. We attribute this to the non-centrosymmetry of the odd shapes, imposing lattices with two NPs in the unit cell in a double-lattice configuration,[9] whereas those of

centrosymmetric nanoparticles (i.e. with even n) have only one NP in the unit cell (**Figure 2B**). Pentagons do not tile the plane, inducing the emergence of more open lattice polymorphs compared to the other shapes. For n<10, the packing fraction of the densest structure evolves significantly with n (i.e. between 0.83 and 0.92) whereas for n≥10, it converges towards 0.84. It is noteworthy that, although these NPs are faceted, for large n the problem converges to the closest packing of perfectly rounded truncated bicones. In this limit (n→∞), the densest phase has a packing fraction of approximately 0.84, but the second densest (and quite frequently occurring) structure, with a packing fraction of 0.77, corresponds to an ellipsoid packing (the densest to date), in which the particles are stacked in alternating layers with differing orientations (**Figure S4.3**).[16] Our results point towards an even denser packing than previously reported for ellipsoids due to the noncircular cross section of the objects. Overall, two regimes for the structuration of faceted bipyramids were identified, depending on n: a "faceted" regime for n<10 and a "smooth" regime for n≥10. Among these different shapes, bipyramids with n=5 exhibit a particularly rich variety of observed structures and low maximum packing, confirming the specificity of the pentagonal cross section.

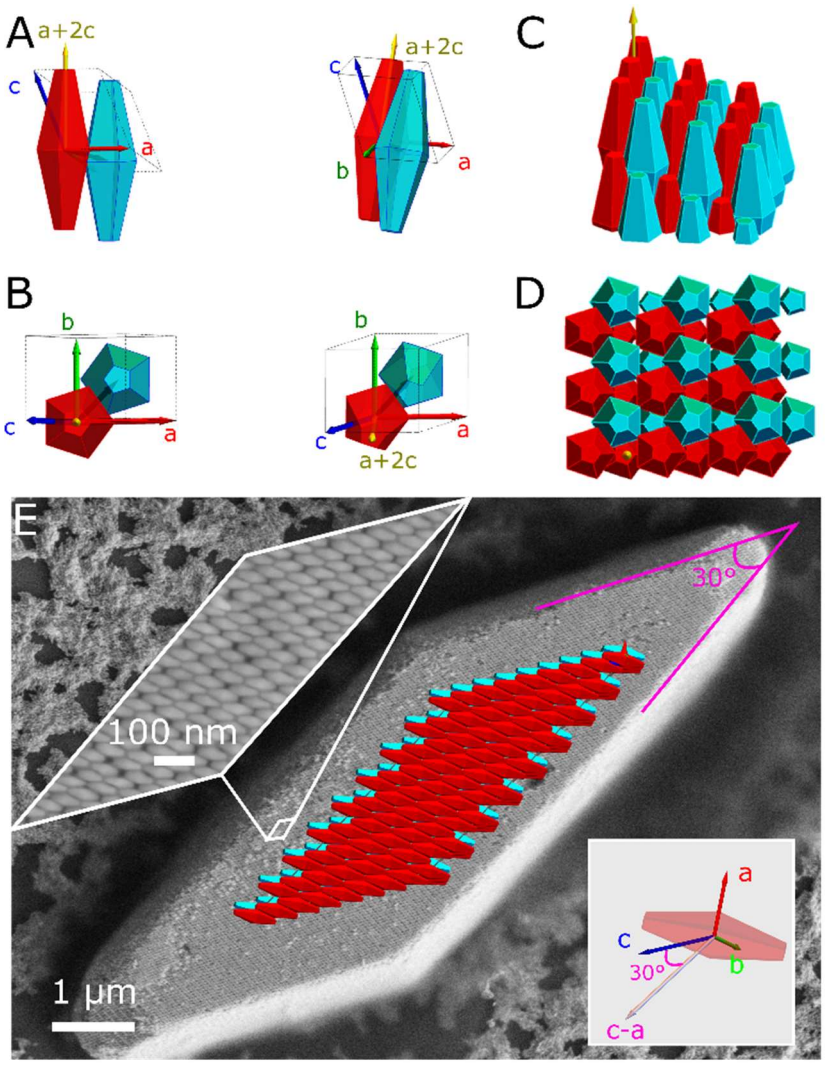

Figure 3: Comparison between the model and the experiment. A-B) P$\bar{1}$ unit cell predicted numerically, composed of two bipyramids drawn in red and blue. C) View of the lattice in which the cut is orthogonal to the [1,0,2] direction. D) Projection of the packing along the [1,0,2] direction (i.e. the longitudinal axis of the bipyramids). E) SEM image of a rhomboidal supercrystal, with superimposed model: both exhibit an angle of 30° at their tips. On top of the supercrystal, the (010) facet forms a rhomboid. The upper inset shows a magnified SEM image of the supercrystal (010) facet, where the bipyramids are lying flat. The lower inset shows the unit cell of the model, oriented along the **c** and **c-a** vectors of the triclinic lattice. 16 mM of Au^0 and 2.5 mM of CTAC were used for sample preparation.

We next compared the simulation results with the experimental analysis in real space (SEM) and in reciprocal space (SAXS). Among the five predicted structures for pentagonal bipyramids, the densest one matched the lattice determined experimentally. In agreement with the simulations, we find a double-lattice arrangement, where all pentagonal bipyramids are parallel to each other but have two different orientations, colored in blue and red in **Figures 2 and 3**. The periodic arrangement is a triclinic lattice with two particles in the unit cell with each type of orientation (**Figure 3A-B**). The two particle orientations are related by an inversion center, so their pentagonal cross-sections are turned by an angle of $\frac{2\pi}{10} = 36°$ (**Figure 3B**). The whole structure can be decomposed into two identical lattices, each one containing all particles with the same orientation (blue or red). The space-group is $P\bar{1}$, with the inversion center located in-between the centers of the two particles in the unit cell, in agreement with the SAXS model. Note that the long axis of the bipyramids is along a direction close to **a+2c**. The structure can also be decomposed in alternate layers with the two orientations (ABA stack), as can be seen from the projection of the structure onto the (**a**,**b**) plane displaying pentagons with the two orientations (**Figure 3D**). We conclude that the supercrystals are oriented along the **c** and **c-a** vectors of the triclinic lattice, by superimposing the model lattice composed of a few NPs on a SEM image of one supercrystal (**Figure 3E**). The agreement between the model and the experiment is very good, as shown by the identical orientation of the particles at the nanoscale and a similar angle of 30° between the micrometer-sized rhomboidal tips and the angle defined by the **c** and **c-a** vectors of the unit cell. The lattice parameters of the triclinic unit cell were found to be a = 41.35 nm; b = 37.24 nm; c = 47.74 nm; α = 105°; β=109°; γ=90° (**Figure S2.9**). The experimental packing fraction was determined as 0.835, in excellent agreement with the one determined from the MC computer simulations (0.83). The triclinic pinacoidal lattice ($P\bar{1}$) defines a low-symmetry architecture ,with only the center inversion as symmetry operation.[24]

To the best of our knowledge, this is the first experimental realization of the shape-directed self-assembly of a triclinic supercrystal.[25]

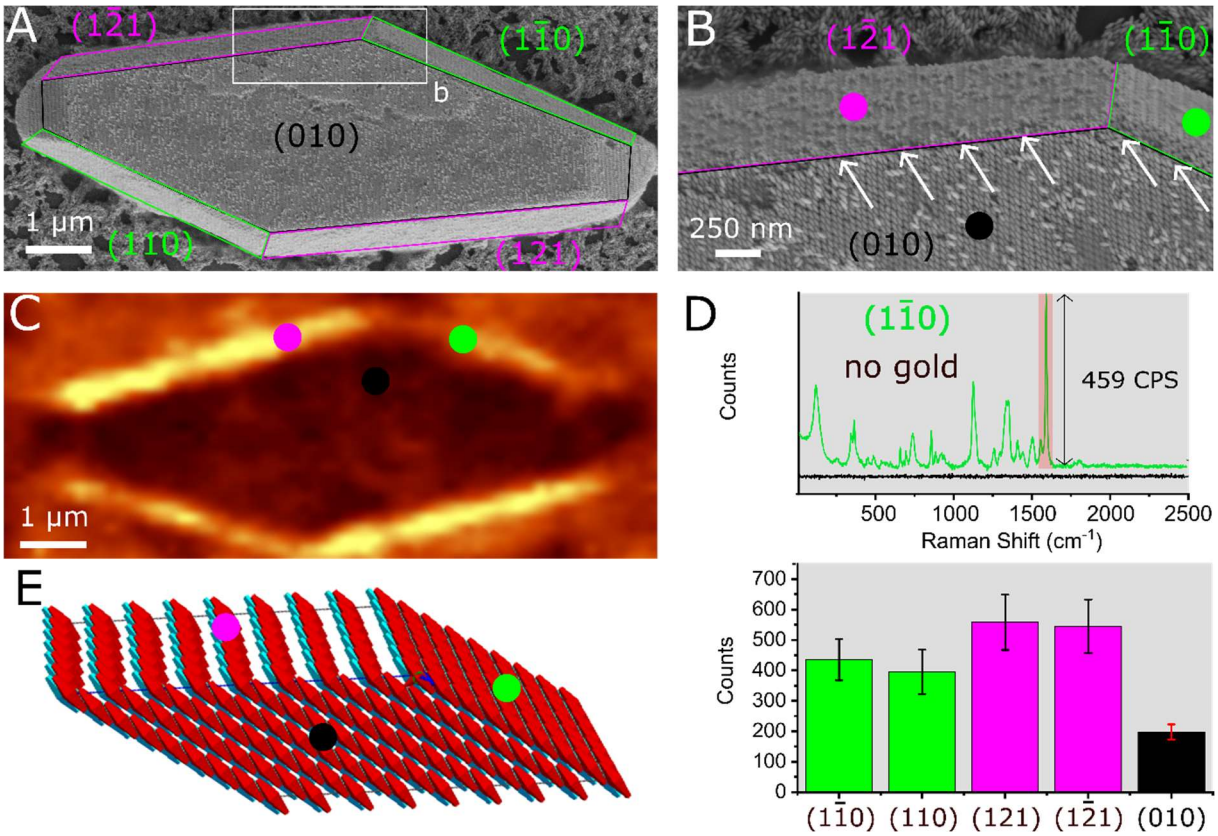

Figure 4: Facet-dependent surface enhanced resonance Raman scattering on a gold bipyramid supercrystal. A-B) SEM micrographs of an AuBPs supercrystal viewed at different magnifications. The largest (010) facet is surrounded by lateral facets. The surface facets of the supercrystal, (1$\bar{2}$1), (1$\bar{1}$0) and (010), are outlined with pink, green and black frames, respectively. C) SERRS image obtained by mapping the intensity of the crystal violet vibrational peak over 1618-1632 cm^{-1}. D) (top) representative SERRS spectrum of crystal violet measured on the (1$\bar{1}$0) facet (green) and Raman spectrum of CV measured without gold in the same experimental conditions (black). The red-shaded area indicates the spectral range integrated for generating the SERRS images in (C). (bottom) histogram of the mean SERRS intensity at 1620 cm^{-1} on the different facets, with the errors bars indicating the standard deviation on each facet. The concentration of CV in the solution was 10^{-6} M, the acquisition

time was 100 ms, and the laser power at the sample was ≈0.1 mW, at an excitation wavelength of 633 nm. E) Model of the triclinic lattice for the supercrystal. The (010) facet is constructed with the edge vectors **c** and **c-a** of the unit cell. The AuBPs are lying flat onto the (010) facet and they are pointing outwards of the $(1\bar{2}1)$ facet.

Finally, the optical properties of the supercrystals were investigated by SERS, allowing the detection of the spectral fingerprint of a probe molecule in contact with the plasmonic surface.[26] As an analyte, we used Crystal Violet (CV), which is resonant with the laser frequency, resulting in surface-enhanced resonance Raman scattering (SERRS). This analysis was performed on a faceted supercrystal (**Figure 4A-B**). The SERRS signal intensity was uniform on each facet due to the periodic arrangement of the nanoparticles (**Figure 4C**). Moreover, the average signal is found to be facet-dependent, with the $(1\bar{2}1)$ facets displaying the highest SERRS intensity (**Figure 4D**). This phenomenon can be ascribed to the varying local arrangement of the NPs on the different facets, directly affecting electromagnetic hotspots formation at the interparticles gaps.[26] The orientation of the longitudinal axis of the bipyramids with respect to the surface plays a key role: When this axis is parallel to the surface facet (i.e. the (010) one), the Raman enhancement is small (201 CPS) whereas a much higher enhancement (560 CPS) is observed when the bipyramids point outwards (i.e. the $(1\bar{2}1)$ facet) (**Figure 4**).[27] In contrast, mapping the SERRS intensity in a similar way on gold nanosphere supercrystals resulted in a uniform response (**Figure S6.4**). Here, we show facet-dependent SERS properties that originate from the anisotropy of the AuBPs, opening an avenue for tailored SERS performance using supercrystals with "spiky" and "smooth" facets, displaying respectively high and low SERS efficiency.

Conclusion

This work shows that fivefold symmetry and anisotropy can be combined to crystallize complex nano-objects into triclinic pinacoidal supercrystals. Pentagonal gold bipyramids pack into

crystals with two particles per unit cell, corresponding to the densest packing predicted by Monte Carlo (MC) computer simulations. Further simulations show how the cross section influences the arrangement (symmetry and packing fraction) of the particles, beyond pentagonal bipyramids. Objects with an odd-sided base are non-centrosymmetric but the two-particle unit cell retrieves inversion symmetry, explaining the double-lattice arrangement. Surprisingly, their packing fraction is lower than that of even-sided particles. The double-lattice packing generalizes the optimal packing of regular pentagons in the plane, the 'pentagonal ice ray' in a non-trivial manner (as can be seen in **Figure 3D**), since the section of the bipyramids is not constant along their long axis. This gold bipyramid supercrystal has a facet-dependent optical response, with spiky and smooth facets displaying respectively high and low SERS efficiency. Its low-symmetry triclinic structure is also useful for metamaterials applications and for fundamental studies of self-assembly processes.

Supporting Information

Supporting Information is available from the Wiley Online Library or from the author.

Acknowledgments

The CNRS is acknowledged for funding and support. The authors thank Claire Goldmann for continuous experimental support and Stéphan Rouzière for the use of the MORPHEUS platform. J. L. acknowledges financial support by the China Scholarship Council (CSC) for her PhD. This work has benefited from an Investissements d'Avenir grant from Labex PALM (ANR-10-LABX-0039-PALM). We acknowledge SOLEIL for the provision of synchrotron radiation facilities (experiment 20201118, SWING beamline). The present work has benefited from the electronic microscopy facility of Imagerie-Gif, (http://www.i2bc.parissaclay.fr), member of IBiSA (http://www.ibisa.net), supported by "France-BioImaging" (ANR10-INBS-04-01), and the Labex "Saclay Plant Science" (ANR-11-IDEX-0003-02).

References:

[1] a) Z. Quan, J. Fang, *Nano Today* **2010**, 5, 390; b) J. Gong, R. S. Newman, M. Engel, M. Zhao, F. Bian, S. C. Glotzer, Z. Tang, *Nat. Commun.* **2017**, 8, 14038; c) P. F. Damasceno, M. Engel, S. C. Glotzer, *Science* **2012**, 337, 453; d) S. Torquato, Y. Jiao, *Nature* **2009**, 460, 876; e) M. H. Huang, S. Thoka, *Nano Today* **2015**, 10, 81; f) C. W. Liao, Y. S. Lin, K. Chanda, Y. F. Song, M. H. Huang, *J. Am. Chem. Soc.* **2013**, 135, 2684; g) J.-M. Meijer, A. Pal, S. Ouhajji, H. N. W. Lekkerkerker, A. P. Philipse, A. V. Petukhov, *Nat. Commun.* **2017**, 8, 14352; h) Y. Nagaoka, R. Tan, R. Li, H. Zhu, D. Eggert, Y. A. Wu, Y. Liu, Z. Wang, O. Chen, *Nature* **2018**, 561, 378; i) Y. Nagaoka, H. Zhu, D. Eggert, O. Chen, *Science* **2018**, 362, 1396; j) H. Lin, S. Lee, L. Sun, M. Spellings, M. Engel, S. C. Glotzer, C. A. Mirkin, *Science* **2017**, 355, 931.

[2] a) D. Frenkel, *Nat. Mater.* **2015**, 14, 9; b) L. Onsager, *Ann. N.Y. Acad. Sci.* **1949**, 51, 627; c) L. Scarabelli, C. Hamon, L. M. Liz-Marzán, *Chem. Mater.* **2017**, 29, 15.

[3] a) C. Zong, *Expositiones Mathematicae* **2014**, 32, 297; b) T. Janssen, A. Janner, *Advances in Physics* **1987**, 36, 519.

[4] J. Kepler, *The harmony of the world*, American Philosophical Society, [Philadelphia, Pa.] **1997**.

[5] M. Rao, 2017, arXiv:1708.00274.

[6] a) D. Schattschneider, *Mathematics Magazine* **1978**, 51, 29; b) J.-F. Sadoc, R. Mosseri, *Geometrical Frustration*, Cambridge University Press, Cambridge **1999**.

[7] a) T. Hales, W. Kusner, 2016, arXiv:1602.07220; b) C. L. Henley, *Phys. Rev. B* **1986**, 34, 797.

[8] D. S. Dye, *A grammar of Chinese lattice / by Daniel Sheets Dye*, Harvard University Press, Cambridge, Mass **1949**.

[9] G. Kuperberg, W. Kuperberg, *Discrete&Computational Geometry* **1990**, 5, 389.

[10] T. Schilling, S. Pronk, B. Mulder, D. Frenkel, *Phys. Rev. E* **2005**, 71, 036138.

[11] a) N. Winckelmans, T. Altantzis, M. Grzelczak, A. Sánchez-Iglesias, L. M. Liz-Marzán, S. Bals, *J. Phys. Chem. C* **2018**, 122, 13522; b) Y. Xia, K. D. Gilroy, H. C. Peng, X. Xia, *Angew. Chem. Int. Ed.* **2017**, 56, 60.

[12] M. Liu, P. Guyot-Sionnest, *J. Phys. Chem. B* **2005**, 109, 22192.

[13] a) A. Sánchez-Iglesias, N. Winckelmans, T. Altantzis, S. Bals, M. Grzelczak, L. M. Liz-Marzán, *J. Am. Chem. Soc.* **2017**, 139, 107; b) D. Chateau, A. Liotta, F. Vadcard, J. R. Navarro, F. Chaput, J. Lermé, F. Lerouge, S. Parola, *Nanoscale* **2015**, 7, 1934.

[14] a) T. Ming, X. Kou, H. Chen, T. Wang, H.-L. Tam, K.-W. Cheah, J.-Y. Chen, J. Wang, *Angew. Chem. Int. Ed* **2008**, 120, 9831; b) Q. Shi, K. J. Si, D. Sikdar, L. W. Yap, M. Premaratne, W. Cheng, *ACS Nano* **2016**, 10, 967.

[15] A. Donev, F. H. Stillinger, P. M. Chaikin, S. Torquato, *Phys. Rev. Lett.* **2004**, 92, 255506.

[16] A. Trovato, T. X. Hoang, J. R. Banavar, A. Maritan, *Proc. Natl. Acad. Sci. U.S.A.* **2007**, 104, 19187.

[17] a) A. Haji-Akbari, M. Engel, S. C. Glotzer, *Phys. Rev. Lett.* **2011**, 107, 215702; b) A. Haji-Akbari, E. R. Chen, M. Engel, S. C. Glotzer, *Phys. Rev. E* **2013**, 88, 012127.

[18] M. J. Solomon, D. V. Boger, *J. Rheol.* **1998**, 42, 929.

[19] a) S. Li, L. Wang, B. Liu, *Soft Matter* **2020**, 16, 8024; b) J. Roller, A. Laganapan, J.-M. Meijer, M. Fuchs, A. Zumbusch, *Proc. Natl. Acad. Sci. U.S.A.* **2021**, 118, e2018072118.

[20] M. N. O'Brien, M. R. Jones, C. A. Mirkin, *Proc. Natl. Acad. Sci. U.S.A.* **2016**, 113, 11717.

[21] a) C. Hamon, M. N. Sanz-Ortiz, E. Modin, E. H. Hill, L. Scarabelli, A. Chuvilin, L. M. Liz-Marzan, *Nanoscale* **2016**, 8, 7914; b) J. E. S. van der Hoeven, E. B. van der Wee, D. A. M. de Winter, M. Hermes, Y. Liu, J. Fokkema, M. Bransen, M. A. van Huis, H. C. Gerritsen, P. E. de Jongh, A. van Blaaderen, *Nanoscale* **2019**, 11, 5304.

[22] L. Filion, M. Marechal, B. van Oorschot, D. Pelt, F. Smallenburg, M. Dijkstra, *Phys. Rev. Lett.* **2009**, 103, 188302.

[23] J. d. Graaf, L. Filion, M. Marechal, R. v. Roij, M. Dijkstra, *J. Chem. Phys.* **2012**, 137, 214101.

[24] D. E. Sands, *Introduction to Crystallography*, (Dover Publications, 2012).

[25] J. Dshemuchadse, 2021, arXiv:2112.07083.

[26] a) J. Langer, D. Jimenez de Aberasturi, J. Aizpurua, R. A. Alvarez-Puebla, B. Auguie, J. J. Baumberg, G. C. Bazan, S. E. J. Bell, A. Boisen, A. G. Brolo, J. Choo, D. Cialla-May, V.

Deckert, L. Fabris, K. Faulds, F. J. Garcia de Abajo, R. Goodacre, D. Graham, A. J. Haes, C. L. Haynes, C. Huck, T. Itoh, M. Kall, J. Kneipp, N. A. Kotov, H. Kuang, E. C. Le Ru, H. K. Lee, J. F. Li, X. Y. Ling, S. A. Maier, T. Mayerhofer, M. Moskovits, K. Murakoshi, J. M. Nam, S. Nie, Y. Ozaki, I. Pastoriza-Santos, J. Perez-Juste, J. Popp, A. Pucci, S. Reich, B. Ren, G. C. Schatz, T. Shegai, S. Schlucker, L. L. Tay, K. G. Thomas, Z. Q. Tian, R. P. Van Duyne, T. Vo-Dinh, Y. Wang, K. A. Willets, C. Xu, H. Xu, Y. Xu, Y. S. Yamamoto, B. Zhao, L. M. Liz-Marzan, *ACS Nano* **2020**, 14, 28; b) S. Schlücker, *Angew. Chem. Int. Ed.* **2014**, 53, 4756.

[27] a) M. Liu, P. Guyot-Sionnest, T.-W. Lee, S. K. Gray, *Phys. Rev. B* **2007**, 76, 235428; b) J. Reguera, J. Langer, D. Jimenez de Aberasturi, L. M. Liz-Marzan, *Chem. Soc. Rev.* **2017**, 46, 3866.